Preparation and Characterization of Antimony-Doped Tin Dioxide Electrodes. Part 1. Electrochemical Characterization

F. Montilla,[†] E. Morallón,*[,†] A. De Battisti,[‡] and J. L. Vázquez[†]

Departamento de Química Física, Universidad de Alicante, Apartado de Correos 99, Alicante, Spain E-03080, and Dipartimento di Chimica, Università degli Studi di Ferrara, Via Borsari 46, 44100 Ferrara, Italy

Received: November 14, 2003; In Final Form: January 20, 2004

Antimony and antimony−platinum doped tin dioxide electrodes supported on titanium have been prepared by thermal decomposition. Ti/SnO_2−Sb electrodes have a cracked-mud structure, typical of oxide electrodes prepared by thermal decomposition. The introduction of platinum in the oxide layer has a packing effect in the coating morphology. The electrochemical characterization of these electrodes has been performed in acid medium, and a relation between the roughness factor (measured from electrode capacitance) and electrochemical porosity (related to the voltammetric charge) has been established. The mechanism for the oxygen evolution reaction has been determined by Tafel measurements indicating that the electrodes prepared are nonactive electrodes. The electrocatalytic activity strongly depends on geometric factors, since the activity toward oxygen evolution increases with the electrochemical porosity. Anodic stability of Ti/SnO_2 electrodes has been checked with accelerated service life tests. The introduction of platinum in the oxide coating increases the service life by 2 orders of magnitude.

1. Introduction

The use of metallic-oxide electrodes for several technological applications is quite new. The development of dimensionally stable anodes (DSA) was promoted by the strong technological demand of the chlorine production industry.[1] These electrodes consist of a titanium substrate covered with an oxide coating, whose composition strongly affects their electrochemical behavior. Thus, RuO_2-based film-electrodes are commonly used for chlorine production,[2−5] but, notwithstanding their good catalytic activity also for the oxygen evolution reaction (OER), they are unsuitable for applications where OER is the anode reaction, because of its very short service life. In fact, IrO_2-based film electrodes perform much better under the latter polarization conditions.[6−8] For applications such as electrochemical oxidation of organic compounds, the electrode material requires a minimal catalytic activity toward the OER and PbO_2 and SnO_2 layers may be used.[9−15] Although stability and electrochemical activity of DSA-type electrodes are largely determined by the nature of the active component, i.e., RuO_2 or IrO_2, considerable improvements can be achieved by adding an adequate promoter.[16−23]

Tin dioxide crystallizes in a rutile-type structure, it is quite inert toward chemical etching with common acid or alkalis and its conductivity can be enhanced by the addition of an appropriate dopant such as In(III), Sb(V), or F^-.[24] The addition of other dopants, such as platinum, osmium, or palladium, introduces some special properties to this oxide coating for its uses in gas sensing devices.[25−28]

The main application of supported SnO_2-film electrodes is the electrochemical incineration of organic compounds in aqueous solutions. The most common dopant for this application is Sb,[9,12,29−31] with Ti being the most reliable metal support. Since this type of electrode presents a high oxygen overpotential, they are very suitable for the electrochemical combustion of organic pollutants.[9−12,32] The main drawback for the use of these electrodes is its extremely low service life under anodic polarization. Several methods have been employed to increase the service life of Sb-doped SnO_2 electrodes: the incorporation of new dopants,[31,33] the introduction of interlayers between the titanium and the active oxide,[34] or the improvement in the preparation method.[11]

The preparation and the characterization of antimony-doped and antimony−platinum-doped SnO_2 electrodes supported on titanium are the objective of this work. Service life tests have been performed in order to check the anodic stability of doped tin oxide layers. A characterization (morphological and electrochemical) of the freshly prepared and deactivated electrodes by service life tests has been performed in order to understand the deactivation mechanism. For these proposes, a morphological study of the deposited layers has been performed by scanning electron microscopy (SEM). The electrochemical properties such as specific capacitance, electrochemical roughness, and electrochemical porosity have been examined by cyclic voltammetry (CV). The electrocatalytic activity toward OER has been studied by quasi-steady polarization curves.

2. Experimental Section

An Autolab PGSTAT 20 system, controlled by GPES EcoChimie software, has been employed for the voltammetric measurements. A platinum wire was employed as the counter-electrode and a saturated calomel electrode (SCE) as the reference electrode. The current density has been calculated using the apparent geometric area of the working electrode (1 cm^2). Stabilized voltammograms have been obtained after 10 scans between the cathodic and the anodic limits. The test-solutions were prepared with water from a Millipore MilliQplus system and they were de-oxygenated by N_2 bubbling. The 0.5M

* To whom correspondence should be addressed. E-mail: morallon@ua.es.
[†] Universidad de Alicante.
[‡] Università degli Studi di Ferrara.

10.1021/jp037480b CCC: $27.50
Published on Web 03/18/2004

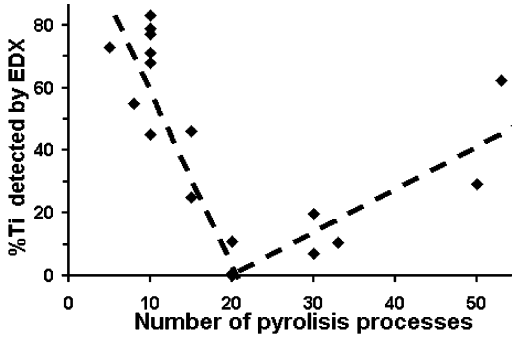

Figure 1. Titanium detected by EDX for several Ti/doped SnO_2 prepared by thermal decomposition as a function of the number of pyrolisis processes.

H_2SO_4 solutions were prepared from the Merck Suprapur concentrated acid.

The surface texture of the electrodes was studied by scanning electron microscopy (SEM Hitachi S-3000N). For the energy dispersive X-ray (EDX) microanalysis of the samples, a Rontec EDX detector coupled to the SEM microscope was employed.

2.1. Preparation of Doped SnO_2 Electrodes. The doped SnO_2 electrodes were prepared following a standard thermal decomposition method. Ti plates ($1 \times 1 \times 0.05$ cm, Goodfellow 99.6%) were used as substrates. Prior to their use as supports, they were degreased with acetone and etched in a boiling 10% oxalic acid solution during 1 h, and after that, they were rinsed with distilled water. Ti/SnO_2−Sb electrodes were prepared using a solution containing 10% $SnCl_4x5H_2O$ (Aldrich) + 1% $SbCl_3$ (Fluka p.a.) dissolved in a mixture of ethanol (Merck p.a.) + HCl (Merck p.a.). The electrodes containing platinum were prepared by adding to the previous solution a precursor of platinum. Two sets of electrodes were prepared by adding H_2PtCl_6 0.4% in weight (3% atom) and 2.1% in weight (13% atom), respectively. The precursor solution was distributed onto the Ti plates by brushing. The solvent was dried in air, and the electrode was introduced in an oven at 400 °C for 10 min for the decomposition of the salt and the formation of the metal oxide. This process was repeated until a number of deposition steps was reached. A final annealing of the electrode was performed at 600 °C for 1 h. The weight of the electrode was measured before and after the deposition process in order to determine the oxide loading.

3. Results and Discussion

3.1. EDX and SEM Characterization. Figure 1 shows the amount of titanium detected by EDX microanalysis against the number of deposition processes. When the number of successive depositions is lower than 20, the EDX response for Ti is high (20−80%). Since the sampling depth of this EDX analysis is at least 1μm, the EDX measurement corresponds to the metal support. When the number of depositions was around 20, the Ti peak decreased below the detection limit of the technique, indicating that, with this level of loadings (oxide loadings around 1.8 mg cm^{-2}), a good coverage of the surface is achieved. Considering the density for SnO_2 (cassiterite), $\rho = 6.95$ g cm^{-3}, the nominal thickness of the deposited layer would be 2.6 μm. Figure 1 shows that, if the number of deposition is increased over 20, titanium is again detected, indicating a worse coverage of the support. This fact can be explained as a partial detachment of the deposited layer when the number of pyrolysis processes increases.

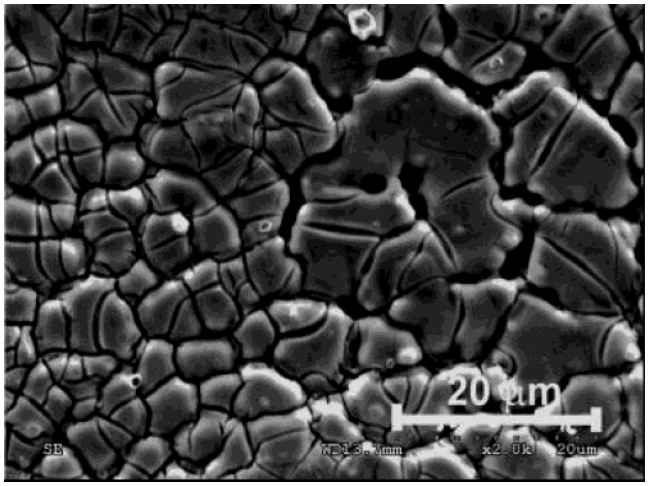

Figure 2. SEM image of a Ti/SnO_2−Sb electrode prepared with 20 pyrolisis processes.

The morphology of the electrodes was followed by SEM. The surface of Ti supports (figure not shown) has a highly disordered and cratered structure after the chemical etching.

Figure 2 shows the SEM image of a Ti/SnO_2−Sb electrode prepared after 20 pyrolysis processes, which presents a typical cracked-mud structure observed with thermally prepared coatings.[35−37] This morphology is similar to that obtained by Lipp and Pletcher,[11] although their electrodes presented a honeycomb substructure that cannot be observed in the present work. Correa-Lozano et al.[38] prepared SnO_2−Sb electrodes on titanium plates by a spray-pyrolysis technique, and they detected these kinds of cracks for a film thickness higher than 1 μm. These cracks are produced on the surface during the cooling of the electrode to room temperature.

The introduction of platinum in the oxide layer significantly affects the coating morphology (Figure 3). As shown in Figure 3a, the surface of a Ti/SnO_2−Sb−Pt(3% atom) film is less cracked. By increasing the Pt concentration up to 13% atom (Figure 3b), the cracks almost disappear from the electrode surface. This compacting effect of platinum was also observed by other authors in SnO_2 thin films prepared by the pyrosol co-deposition method.[39]

3.2. Electrode Stability. The main problem for using tin dioxide electrodes is its short service life in anodic polarization conditions in aqueous media. The accelerated service life tests were performed by anodic polarization of the different electrodes at 1 A cm^{-2} in a 0.5 M H_2SO_4 solution. The anode potential was measured as a function of time, and it was considered that the electrode is deactivated when the potential overcomes 5 V from its initial value. Table 1 summarizes the service life for different electrodes, expressed as efficiency, that is, total charge passed (Ampere hour) per mg of deposited oxide (Ah mg^{-1}).[7] The introduction of platinum in the oxide layer improves the service life by 1 or 2 orders of magnitude. The Ti/SnO_2−Sb−Pt(3% atom) electrodes shows the best performance; however, higher amounts of platinum (13% atom) decrease these results.

The best performance is obtained with 20 deposition processes for all electrode compositions. A subsequent increase of the number of deposition processes does not improve the service life of these electrodes due to the poorer coverage of the titanium support.

3.3. Cyclic Voltammetry and Capacitance Measurements. The cyclic voltammogram of a Ti/SnO_2−Sb electrode in a 0.5 M H_2SO_4 solution does not show remarkable voltammetric features, and only capacitive currents can be observed in the

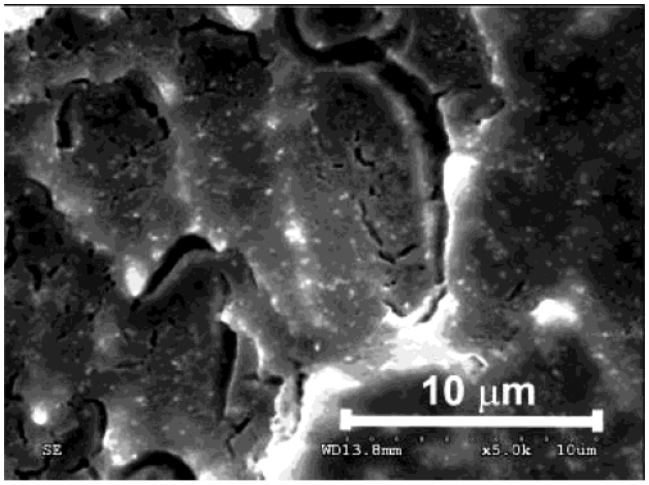

a

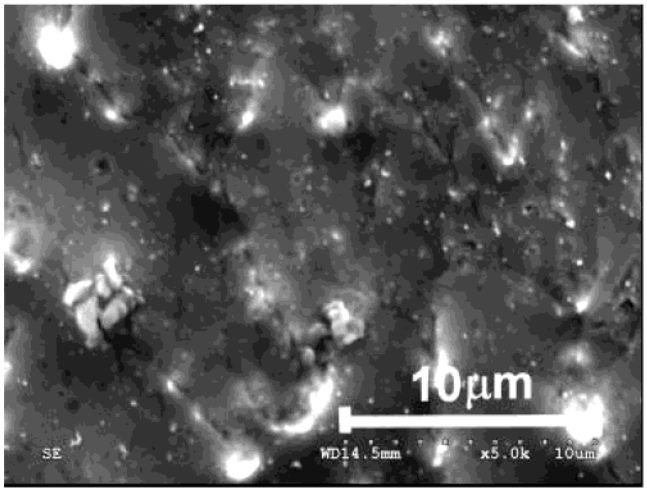

b

Figure 3. SEM images of $Ti/SnO_2-Sb-Pt$ electrodes prepared with 20 pyrolisis processes: (a) $Ti/SnO_2-Sb-Pt$(3% atom); (b) $Ti/SnO_2-Sb-Pt$(13% atom).

TABLE 1: Service Life in the Accelerated Test Performed at 1 A cm^{-2} in a 0.5 M H_2SO_4 Solution for Several Ti/Doped SnO_2 Electrodes with and without Platinum[a]

platinum content (% atom)	deposition process	service life (efficiency, Ah mg^{-1})
0	10	3.6
	20	6.3
	30	1.0
3	10	94.0
	20	284.2
	30	161.4
13	10	24.6
	20	154.2
	30	36.4

[a] Service life is expressed as efficiency, that is, total charge passed (ampere hour) per mg of deposited oxide.

potential range between 0.3 and 1.5 V (Figure 4). The anodic current rises at potentials more positive than 1.5 V due to the OER. The cathodic current appears at potentials less positive than 0.3 V, due to the irreversible reduction of the tin oxide, which produces electrode damage. For this reason, the lower potential limit must not be fixed below 0.3 V.[31,33,40]

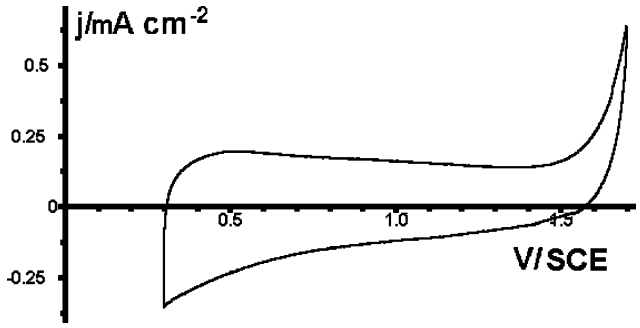

Figure 4. Stabilized cyclic voltammogram of a Ti/SnO_2-Sb electrode in a 0.5M H_2SO_4 solution. $\nu = 50$ mV s^{-1}.

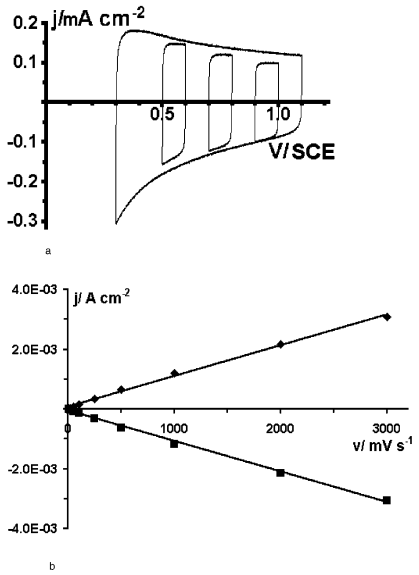

Figure 5. a) Cyclic voltammograms of a Ti/SnO_2-Sb electrode in a 0.5M H_2SO_4 solution between 0.3 and 1.1 V (CV) and in three shorter ranges of potential (DV). $\nu = 100$ mV s^{-1}. (b) Evolution of the current density at 0.55V against the potential scan rate measured in the DV between 0.5 and 0.6 V for a Ti/SnO_2-Sb electrode in a 0.5 M H_2SO_4 solution. Potential scan rate range from 10 to 3000 mV s^{-1}.

Capacitance measurements have been performed in order to determine the roughness factor (R_f) of the different electrodes. Figure 5a shows the cyclic voltammogram obtained between 0.3 and 1.1 V at a scan rate of 100 mV s^{-1} (complete voltammogram, CV) and the voltammograms obtained at the same scan rate but in three narrower potential ranges with $\Delta E = 0.1$ V (differential voltammogram, DV[41]). The differences between currents measured in the complete, CV, and the differential, DV, voltammograms could be associated to some hysteresis phenomena like charge accumulation or slow capacitive processes.[41]

The values of capacitance have been measured in the DV from the cathodic and anodic current densities in the midpoint of the potential range (0.55, 0.75, and 0.95 V) for several scan rates. Figure 5b shows the plot of the cathodic and anodic current densities obtained at 0.55 V versus the scan rate. Similar plots were obtained at 0.75 and 0.95 V. The linear relationship between current density and scan rate confirms the nonfaradic character of the current in this zone of potentials between 0.3 and 1.1 V. The capacitance at each potential is obtained from the absolute value of the slopes of the linear plots. Table 2 shows the values of capacitance obtained for different Ti/SnO_2-Sb electrodes prepared with 10, 20, and 30 deposition processes. It can be observed that the capacitance decreases as the potential increases. This trend is predicted by the Mott−Schottky

TABLE 2: Capacitance at Three Potentials, Mass Capacitance at 0.55 V, and Roughness Factor Calculated at 0.55 V for Several Ti/Doped SnO_2 Electrodes with and without Platinum Calculated from the Voltammetric Measures of Capacitance in a 0.5 M H_2SO_4 Solution[a]

platinum content (% atom)	no. of deposition processes	capacitance (mF cm^{-2}) 0.55 (V)	0.75 (V)	0.95 (V)	mass capacitance (F g^{-1})	roughness factor, Rf
0	10	1.06	0.84	0.73	1.51	133
	20	1.31	1.08	0.90	1.03	164
	30	2.17	1.46	1.29	1.09	271
3	10	1.46	1.22	1.14	2.90	183
	20	2.70	2.38	2.24	2.13	338
	30	5.03	4.32	4.12	3.59	629
13	10	3.89	2.87	2.79	2.99	486
	20	5.12	4.39	3.83	2.69	640
	30	9.52	8.03	7.31	2.88	1190

[a] Mean values obtained from several electrodes.

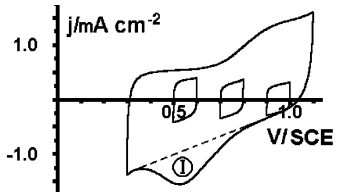

Figure 6. Cyclic voltammograms of a Ti/SnO_2−Sb−Pt(3% atom) electrode in a 0.5 M H_2SO_4 solution between 0.3 and 1.1 V (CV) and in three shorter ranges of potential (DV, 0.5−0.6 V; 0.7−0.8 V; 0.9−1.0 V). $\nu = 100$ mV s^{-1}.

relationship for *n* type semiconductors.[42] Table 2 also shows the mass capacitance calculated from the value at 0.55 V and the oxide loading per square centimeter. The values are of the same order of magnitude than those measured by Wu et al.[43] for Sb-doped SnO_2 electrochemical capacitors prepared at 600 °C.

The roughness factor (R_f) defined as real surface area per apparent geometric area of electrode has been calculated according to Wu et al. using a specific capacitance of 8 μF cm^{-2}.[43] The roughness factor calculated at 0.55V is also shown in Table 2. As the number of deposition processes increases, R_f increases, similar to other electrodes with a rutile-type crystalline structure.[5]

Similar experiments were performed with SnO_2−Sb electrodes doped with platinum. Figure 6 shows the cyclic voltammograms between 0.3 and 1.1 V for a Ti/SnO_2−Sb−Pt(3% atom) electrode in a 0.5 M H_2SO_4 solution. For the electrodes containing platinum, an oxidation current at potentials more positive than 0.7 V is observed due to the oxidation of the platinum surface. The cathodic peak at around 0.5 V corresponds to the reduction of the platinum oxides formed in the positive scan. As the amount of platinum increases, the total electric charge involved in the voltammograms increases proportionally, indicating that there is not surface segregation to a significant extent.

Figure 6 also shows the differential voltammograms (DV) performed in the same ranges of potential than in the case of Ti/SnO_2−Sb electrodes in order to avoid the pseudo-capacitance phenomena, which in the case of Pt-containing electrodes are caused by the oxidation and reduction of the platinum surface. If the limits in the DV are properly selected, the measured currents are related only to the purely capacitance phenomena. Table 2 shows the values of capacitance, mass capacitance, and roughness factor for platinum doped electrodes with two different amounts of platinum and for a different number of deposition processes. The values of mass capacitance and roughness factors obtained are around 2−3 times higher than those of electrodes without platinum, which suggests an increase of the surface area exposed to the solution. Nonetheless, changes of specific capacitance per unit effective area cannot be ruled out.

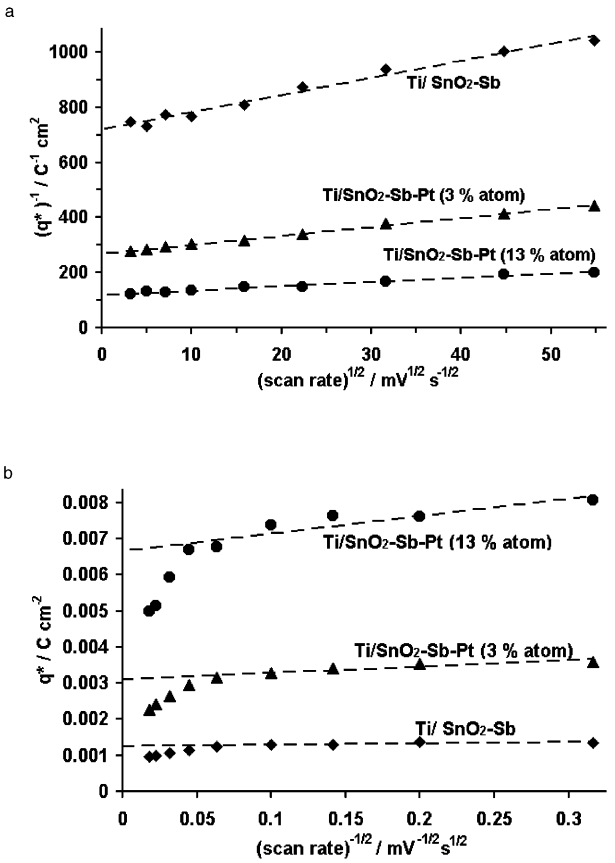

Figure 7. (a) Reciprocal voltammetric charge $(q^*)^{-1}$ versus the square root of the voltammetric scan rate ($\nu^{1/2}$) for three electrodes of different composition for the extrapolation of q_T^*. b) Voltammetric charge (q^*) versus the reciprocal square root of the voltammetric scan rate ($\nu^{-1/2}$) for three electrodes of different composition, for the extrapolation of q_o^*. Data obtained from the cyclic voltammograms with the conditions of Figure 6.

3.4. Voltammetric Charge Analysis. The voltammetric charge (q^*) is related to the real surface area but is also affected by the specific electroactivity of the sites, which depends on the chemical composition of the layers. The voltammetric charge q^* decreases with increasing the potential scan rate for all of the investigated electrode materials (figure not shown), which can be due to some hindered exchange of charged components between the solution and electroactive sites in less accessible parts of the film surface.[2,8] At very low scan rates ($\nu \rightarrow 0$), the total electrochemically active surface takes part in the charging process.

The voltammetric charge corresponding to the total surface area (q_T^*) can be obtained plotting the reciprocal of q^* against the square root of the potential scan rate by using the following equation:[2,44]

$$(q^*)^{-1}(\upsilon) = (q_T^*)^{-1} + k\nu^{1/2} \qquad (1)$$

Figure 7a shows these plots for different doped SnO_2 electrodes. A good linear fitting is observed. The voltammetric charge q_T^*, obtained by extrapolation of the linear plots to $\nu = 0$, increases

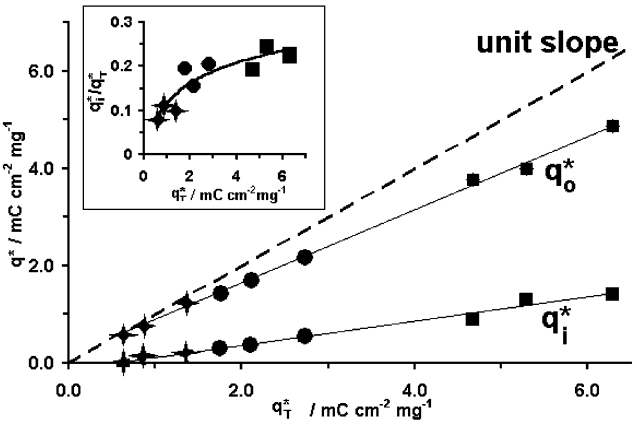

Figure 8. Evolution of the outer (q_o^*) and inner (q_i^*) voltammetric charge as a function of the total voltammetric charge for several Ti/doped SnO_2 electrodes. (◆, rhombus points) Ti/SnO_2−Sb electrodes, (●, circle points) Ti/SnO_2−Sb−Pt(3% atom), and (■, square points) Ti/SnO_2−Sb−Pt(13% atom). Inset: Electrochemical porosity (q_i/q_T) versus the total voltammetric charge.

with the amount of platinum in the oxide coating. Taking into account that the increase of Pt concentration in the electrode film can cause an increase of the effective surface area and of electrical conductivity, the above effect is not surprising.

The values of outer charge, q_o^*, that is, the voltammetric charge related to the electroactive sites which are more accessible to the exchange of charged species between the solution and electrode films, can be obtained from the extrapolation to $\nu \rightarrow \infty$ in the plot of q^* versus $\nu^{-1/2}$ (Figure 7b) according to the following equation[2]

$$q^*(\nu) = q_o^* + k'\nu^{-1/2} \tag{2}$$

The outer voltammetric charge q_o^* increases with the amount of platinum. The extrapolation of this plot is more complicated because at high scan rates there is spurious decreases of the voltammetric charge as a consequence of some interfering factors such as uncompensated ohmic drops in the oxide layer or across the Ti|active oxide interface[45−47] or the irreversibility of the redox reaction on the electrode surface.[8,46,48] As can be observed in Figure 7b, this decrease in the voltammetric charge is more pronounced for electrodes containing platinum due to the irreversibility of the oxidation and reduction of the platinum surface. For potential scan rates lower than 500 mV s^{-1} the reduction peak of the platinum oxides is centered at around 0.5 V and is well defined in the potential range selected (peak I in Figure 6). As the scan rate increases, this reduction peak shifts toward less positive potentials and part of the voltammetric charge of this peak would appear at potentials below the cathodic potential limit of 0.3 V. Similar problems were reported by De Pauli and Trasatti for electrodes of SnO_2 doped with Ir.[8]

From q_T^* and q_o^* data, the inner voltammetric charge (q_i^*) contribution of less accessible surface sites of the oxide layer to the total charge can be calculated

$$q_T^* = q_i^* + q_o^* \tag{3}$$

Figure 8 shows the plot of the outer and the inner voltammetric charge obtained for several electrodes with and without platinum as a function of the total voltammetric charge. The outer charge (q_o^*) increases linearly with the total charge, which has been related with the amount of platinum. The same trend has been observed with other electrodes of metallic oxides.[2,8] The inset of Figure 8 shows the electrochemical porosity defined as the relation between the inner and the total charge (q_i^*/q_T^*) as a function of the total charge (i.e., the amount of platinum). These plots indicate that the electrodes containing platinum have a higher electrochemical porosity.

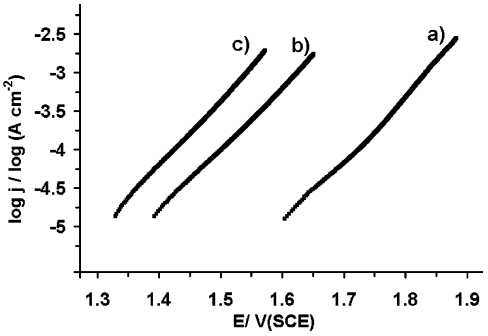

Figure 9. Tafel plots for the oxygen evolution reaction in a 0.5 M H_2SO_4 solution for three electrodes of different composition: (a) Ti/SnO_2−Sb; (b) Ti/SnO_2−Sb−Pt(3% atom); (c) Ti/SnO_2−Sb−Pt(13% atom). The electrodes were preconditioned for 15 min at +3 mA cm^{-2}. Scan rate 1 μA s^{-1}.

As could be observed by SEM, Ti/SnO_2−Sb electrodes show a cracked-mud morphology (Figure 2). The voltammetric analysis indicates that the electrolyte easily diffuses through the cracks of the oxide layer and the inner surface charge (q_i^*) in the Ti/SnO_2−Sb is very small (around 10% of the total active sites). On the other hand, Pt-containing electrodes exhibit a more compact texture (Figure 3). In accordance with this morphological evidence, the electrolyte diffusion through the near-surface region is less fast, and the inner surface charge contribution is more important (around 20%).

3.5. Tafel Slope Measurements. The study of the oxygen evolution reaction in 0.5 M H_2SO_4 solution on doped SnO_2 electrodes has been performed by quasi-steady galvanostatic curves at current densities lower than 3 mA cm^{-2}. Prior to the galvanostatic experiments, the electrodes were conditioned applying 3 mA cm^{-2} for 15 min. This pretreatment produces a completely oxidized surface, more stable during the successive scan. A plot of log j versus potential, known as the Tafel plot, is useful for evaluating kinetic parameters. In general, the slope for an anodic process is $(1 - \alpha)nF/2.3RT$, with α being the transfer coefficient and n being the number of electrons involved in the rate-determining step.[49] Figure 9 shows the Tafel plot obtained from the current potential curves (polarization curves) for the three electrodes [Ti/SnO_2−Sb, Ti/SnO_2−Sb−Pt(3%, atom), and Ti/SnO_2−Sb−Pt(13% atom)]. As expected, the electrocatalytic activity toward OER is higher for the electrodes containing platinum. The log(j) versus potential plots exhibit a sufficiently extended linear part, whose slope is 111 mV for Ti/SnO_2−Sb electrodes, 122 mV for Ti/SnO_2−Sb−Pt(3% atom), electrodes and 115 mV for Ti/SnO_2−Sb−Pt(13% atom) electrodes. These values are close to 120 mV, which correspond to a single electron transfer suggesting a kinetic control by the adsorption of OH from water according to the generally proposed mechanism in the oxygen evolution reaction.[50] The comparison of the electrocatalytic activity toward OER can be easily carried out because of the substantial parallelism of the Tafel plots. The well-known poor catalytic activity of SnO_2-film electrodes is confirmed by plots in Figure 9 which show that small additions of Pt sharply decrease the potential values at constant current density.

So, there are two factors governing the electrocatalytic activity of these electrodes: electronic and geometric factors. Related

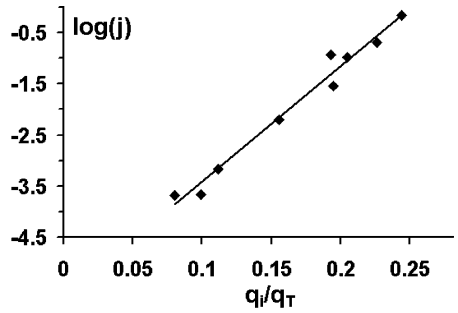

Figure 10. Electrocatalytic activity (log *j*) at +1.8 V/SCE for several Ti/doped SnO_2 electrodes for oxygen evolution reaction in a solution 0.5 M H_2SO_4 against its electrochemical porosity.

with electronic factors (i.e., with the chemical composition of the electrode) when the amount of platinum in the layer increases the electrocatalytic activity also increases (Figure 9).

With respect to the geometrical factors, the electrocatalytic performance of these electrodes toward OER has been evaluated by the measurement of the current density at a constant potential of +1.8 V/SCE for different SnO_2 electrodes. Figure 10 contains the plot between log(*j*) and the electrochemical porosity (q_i^*/q_T^*), in which a linear relation between both parameters can be observed. This result indicates that the electrodes with high inner surface present higher activity for OER, possibly due to an enhanced reactivity in less accessible sites of the active oxide like pores or grain borders. Therefore, in these kinds of electrodes, the morphological factors also have great importance.

4. Effect of the Electrode Deactivation on the Morphology and the Electrochemical Behavior

Figure 11.a shows the SEM micrograph of a Ti/SnO_2−Sb electrode after the service life tests by anodic polarization. When this image is compared with that obtained for a freshly prepared electrode (Figure 2), a clear higher cracking of the surface and a decrease in the size of the oxide plates can be observed. EDX analysis of deactivated electrodes showed a similar composition than the fresh electrode, which indicates that the deactivation is not due to dissolution or detachment of the oxide layer but to the passivation of one of the interfaces implied in the working mechanism of the electrode, i.e., support|active oxide or active oxide|electrolyte solution.[51] Some authors have considered that the deactivation of the electrodes is due to the formation of a passive hydration layer over the SnO_2 that blocks the charge transfer for the OER.[30]

To check this possibility, the electrochemical characterization of deactivated electrodes was performed in a similar way than to the fresh electrodes. Figure 11b shows the cyclic voltammogram of a deactivated Ti/SnO_2−Sb electrode. At potentials between 0.3 and 1.4 V, the shape of the voltammogram is similar to that of a fresh electrode. Only at potentials more positive than 1.4 V can some remarkable differences between both voltammograms be observed. The OER appears at higher potentials in the deactivated electrode, and the shape of the voltammogram in that zone of potentials (the bend of the voltammogram at potentials more positive than 1.7 V) indicates some resistance to the charge transfer.

Capacitance measurements were performed with the deactivated electrodes by measuring the current density of the differential voltammograms (DV) at the same selected middle potentials (0.55, 0.75, and 0.95 V) as in the way than for fresh electrodes. Plots of *j* against scan rate (ν) are linear (figure not shown) in all of the scan rate range (10−3000 mV s^{-1}), which indicates that the deactivated electrodes have activity for the

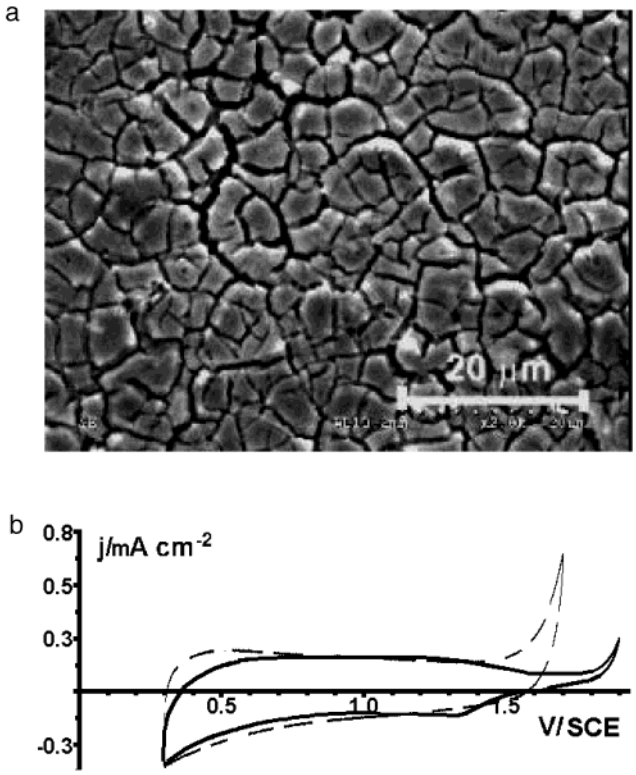

Figure 11. (a) SEM image of a deactivated Ti/SnO_2−Sb electrode after the accelerated service life test. (b) Cyclic voltammogram for a deactivated Ti/SnO_2−Sb electrode in a 0.5 M H_2SO_4 solution. Dashed line: voltammogram for a fresh Ti/SnO_2−Sb electrode in a 0.5 M H_2SO_4 solution. $\nu = 100$ mV s^{-1}.

capacitive charge transfer. In addition, the roughness factors (R_f) measured in the deactivated Ti/SnO_2−Sb electrodes without platinum are slightly higher than the values obtained for fresh electrodes. These results indicate that the charge transfer between the titanium support and the oxide layer is not impeded (capacitive charge); however, there are problems for the charge transfer of faradic character from the oxide layer to the solution, i.e., OER, indicating the passivation of the external interface.

Figure 12a shows the SEM image of a Ti/SnO_2−Sb−Pt(13% atom) electrode after the service life test. The appearance of fractures on the surface can be detected (compare this image with that of Figure 3b obtained for a fresh electrode). The edges of these fractures seem to be oriented outside of the surface oxide, which suggests the breaking of the surface by the action of the emerging oxygen bubbles from inside of the layer produced during the anodic polarization of the electrode. Similar interpretation can be done from the images of the deactivated Ti/SnO_2−Sb−Pt(3% atom) electrode (figure not shown).

Figure 12b shows the cyclic voltammogram for a Ti/SnO_2−Sb−Pt electrode after the service life test. The voltammogram is characterized by the presence of an oxidation current that starts at 0.7 V due to the oxidation of platinum particles, as in the fresh electrodes (Figure 6). No current due to the OER, even at potentials more positive than 1.6 V, can be observed. In the reverse scan, a strong reduction peak is shown at 0.45 V due to the reduction of platinum surface that has been extensively oxidized during the service life test. In contrast with the electrodes of Ti/SnO_2−Sb, the measurements of capacitance for the deactivated Ti/SnO_2−Sb−Pt electrodes from the DV is not possible to perform, since the plot of the current densities against the scan rate is not linear, which shows the absence of good capacitive charge transfer between the titanium support and the oxide layer. These results contrast with those obtained with the

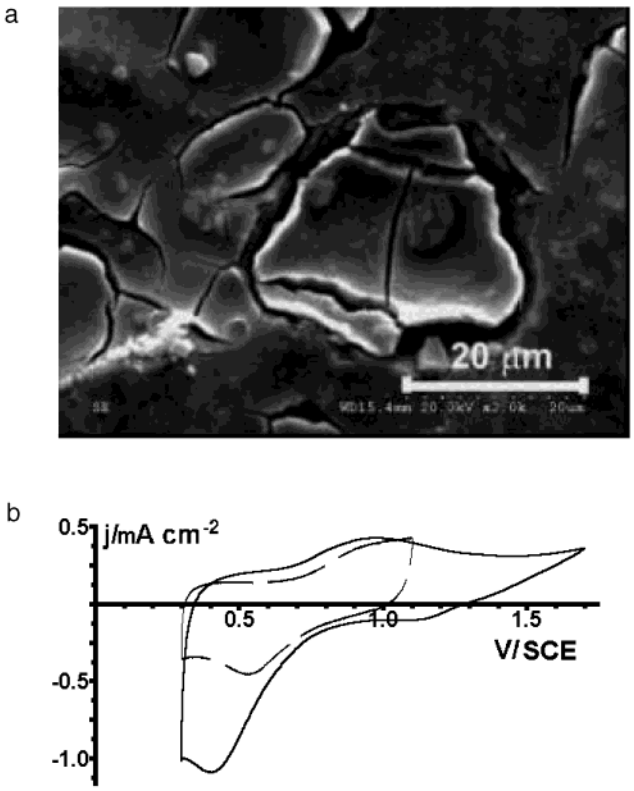

Figure 12. (a) SEM image of a deactivated $Ti/SnO_2-Sb-Pt$(13% atom) electrode. (b) Cyclic voltammogram for a deactivated $Ti/SnO_2-Sb-Pt$(13% atom) electrode in a 0.5 M H_2SO_4 solution. Dashed line: voltammogram for a fresh $Ti/SnO_2-Sb-Pt$(13% atom) electrode in a 0.5 M H_2SO_4 solution. $\nu = 100$ mV s^{-1}.

electrodes without platinum in which the deactivated interface corresponds to the external layer.

5. Conclusions

Doped tin dioxide electrodes have been prepared by thermal decomposition of chloride precursors. These electrodes were characterized by SEM and cyclic voltammetry. The electrodes of Ti/SnO_2-Sb present a cracked-mud structure typical of electrodes prepared by thermal decomposition. The introduction of platinum in the oxide layer produces a change in the morphology because of the compacting effect of the platinum.

The service life of the Ti/SnO_2-Sb electrodes has been strongly increased (up to 2 orders of magnitude) by the addition of small amounts of platinum in the oxide layer (around 3% atom).

The voltammetric behavior of Ti/SnO_2-Sb electrodes shows capacitive currents in the potentials between 0.3 and 1.1 V. The voltammogram for the electrodes containing platinum shows additional currents due to the oxidation and reduction of the platinum surface (pseudo-capacitance phenomena). The real surface area has been determined by capacitance measurements. The roughness factor of the electrodes increases when platinum is introduced in the layer.

The electrochemical activity of these electrodes for the oxygen evolution reaction is strongly dependent on morphological factors. Electrodes containing platinum have higher activity toward OER because of both electronic and geometric factors.

The main cause for the deactivation of Ti/SnO_2-Sb seems to be the formation of a passive layer in the external interface of the electrode, since capacitive charge transfer is not impeded. The introduction of platinum in the layer composition modifies the capacitance properties of the deactivated electrodes, and then, the mechanism of deactivation would be different than the electrodes without platinum. It is necessary to use other techniques for characterizing the electrodes in order to deepen in the mechanism of their deactivation.

Acknowledgment. Financial support by the Generalitat Valenciana (GV01-313) and Ministerio de Ciencia y Tecnología (MAT2001-1007) projects are gratefully acknowledged.

References and Notes

(1) Trasatti, S. *Electrochim. Acta* **2000**, *45* (15−16), 2377−2385.
(2) Ardizzone, S.; Fregonara, G.; Trasatti, S. *Electrochim. Acta* **1990**, *35* (1), 263−267.
(3) Arikawa, T.; Murakami, Y.; Takasu, Y. *J. Appl. Electrochem.* **1998**, *28* (5), 511−516.
(4) Barison, S.; Barreca, D.; Daolio, S.; Fabrizio, M.; Piccirillo, C. *Rapid Commun. Mass Spectrom.* **2000**, *14* (14), 1179−1183.
(5) Burke, L. D.; Murphy, O. J. *J. Electroanal. Chem.* **1979**, *96* (1), 19−27.
(6) Benedetti, A.; Polizzi, S.; Riello, P.; Debattisti, A.; Maldotti, A. *J. Mater. Chem.* **1991**, *1* (4), 511−515.
(7) Comninellis, C.; Vercesi, G. P. *J. Appl. Electrochem.* **1991**, *21* (4), 335−345.
(8) Depauli, C. P.; Trasatti, S. *J. Electroanal. Chem.* **1995**, *396* (1−2), 161−168.
(9) Comninellis, C.; Pulgarin, C. *J. Appl. Electrochem.* **1993**, *23* (2), 108−112.
(10) Grimm, J. H.; Bessarabov, D. G.; Simon, U.; Sanderson, R. D. *J. Appl. Electrochem.* **2000**, *30* (3), 293−302.
(11) Lipp, L.; Pletcher, D. *Electrochim. Acta* **1997**, *42*.(7), 1091−1099.
(12) Stucki, S.; Kotz, R.; Carcer, B.; Suter, W. *J. Appl. Electrochem.* **1991**, *21* (2), 99−104.
(13) Ho, C. C.; Chan, C. Y.; Khoo, K. H. *J. Chem. Technol. Biotechnol.* **1986**, *36* (1), 7−14.
(14) Kawagoe, K. T.; Johnson, D. C. *J. Electrochem. Soc.* **1994**, *141* (12), 3404−3409.
(15) Wendt, H.; Bitterlich, S.; Lodowicks, E.; Liu, Z. *Electrochim. Acta* **1992**, *37* (11), 1959−1969.
(16) Daolio, S.; Kristof, J.; Piccirillo, C.; Pagura, C.; Debattisti, A. *J. Mater. Chem.* **1996**, *6* (4), 567−571.
(17) Endo, K.; Katayama, Y.; Miura, T.; Kishi, T. *J. Appl. Electrochem.* **2002**, *32* (2), 173−178.
(18) Ito, M.; Murakami, Y.; Kaji, H.; Yahikozawa, K.; Takasu, Y. *J. Electrochem. Soc.* **1996**, *143* (1), 32−36.
(19) Kodintsev, I. M.; Trasatti, S.; Rubel, M.; Wieckowski, A.; Kaufher, N. *Langmuir* **1992**, *8* (1), 283−290.
(20) Kotz, R.; Stucki, S. *Electrochim. Acta* **1986**, *31* (10), 1311−1316.
(21) Kristof, J.; Liszi, J.; De Battisti, A.; Barbieri, A.; Szabo, P. *Mater. Chem. Phys.* **1994**, *37* (1), 23−28.
(22) Nanni, L.; Polizzi, S.; Benedetti, A.; De Battisti, A. *J. Electrochem. Soc.* **1999**, *146* (1), 220−225.
(23) Tomcsanyi, L.; Molnar, F.; Liszi, J.; De Battisti, A. *Electrochim. Acta* **1994**, *39* (11−12), 1923−1926.
(24) Chopra, K. L.; Major, S.; Pandya, D. K. *Thin Solid Films* **1983**, *102* (1), 1−46.
(25) Licciulli, A.; Mazzarelli, S.; De, G.; Siciliano, P.; Vasanelli, L.; Rella, R. *J. Sol−Gel Sci. Technol.* **2001**, *21* (3), 195−201.
(26) Chung, W. Y.; Lee, D. D.; Sohn, B. K. *Thin Solid Films* **1992**, *221* (1−2), 304−310.
(27) Gaidi, M.; Labeau, M.; Chenevier, B.; Hazemann, J. L. *Sens. Actuators B−Chem.* **1998**, *48* (1−3), 277−284.
(28) Watson, J.; Ihokura, K.; Coles, G. S. V. *Measurement Sci. Technol.* **1993**, *4* (7), 711−719.
(29) CorreaLozano, B.; Comninellis, C.; De Battisti, A. *J. Appl. Electrochem.* **1996**, *26* (1), 83−89.
(30) Kotz, R.; Stucki, S.; Carcer, B. *J. Appl. Electrochem.* **1991**, *21* (1), 14−20.
(31) Vicent, F.; Morallon, E.; Quijada, C.; Vazquez, J. L.; Aldaz, A.; Cases, F. *J. Appl. Electrochem.* **1998**, *28* (6), 607−612.
(32) Johnson, D. C.; Feng, J.; Houk, L. L. *Electrochim. Acta* **2000**, *46* (2−3), 323−330.
(33) Chen, G. H.; Chen, X. M.; Yue, P. L. *J. Phys. Chem. B* **2002**, *106* (17), 4364−4369.
(34) CorreaLozano, B.; Comninellis, C.; De Battisti, A. *J. Appl. Electrochem.* **1997**, *27* (8), 970−974.
(35) da Silva, L. A.; Alves, V. A.; de Castro, S. C.; Boodts, J. F. C. *Colloids Surf. A-Physicochem. Eng. Aspects* **2000**, *170* (2−3), 119−126.
(36) Forti, J. C.; Olivi, P.; de Andrade, A. R. *Electrochim. Acta* **2001**, *47* (6), 913−920.

(37) Shieh, D. T.; Hwang, B. J. *Electrochim. Acta* **1993**, *38* (15), 2239−2246.
(38) CorreaLozano, B.; Comninellis, C.; De Battisti, A. *J. Electrochem. Soc.* **1996**, *143* (1), 203−209.
(39) Matko, I.; Gaidi, M.; Chenevier, B.; Charai, A.; Saikaly, W.; Labeau, M. *J. Electrochem. Soc.* **2002**, *149* (8), H153−H158.
(40) CorreaLozano, B.; Comninellis, C.; De Battisti, A. *J. Appl. Electrochem.* **1996**, *26* (7), 683−688.
(41) Oren, Y.; Soffer, A. *J. Electroanal. Chem.* **1985**, *186* (1−2), 63−77.
(42) Bott, A. W. *Curr. Separations* **1998**, *17* (3), 87−91.
(43) Wu, N. L.; Hwang, J. Y.; Liu, P. Y.; Han, C. Y.; Kuo, S. L.; Liao, K. H.; Lee, M. H.; Wang, S. Y. *J. Electrochem. Soc.* **2001**, *148* (6), A550-A553.
(44) Vogt, H. *Electrochim. Acta* **1994**, *39* (13), 1981−1983.
(45) Baronetto, D.; Krstajic, N.; Trasatti, S. *Electrochim. Acta* **1994**, *39* (16), 2359−2362.
(46) Baronetto, D.; Kodintsev, I. M.; Trasatti, S. *J. Appl. Electrochem.* **1994**, *24* (3), 189−194.
(47) Spinolo, G.; Ardizzone, S.; Trasatti, S. *J. Electroanal. Chem.* **1997**, *423* (1−2), 49−57.
(48) De Pauli, C. P.; Trasatti, S. *J. Electroanal. Chem.* **2002**, *538* 145−151.
(49) Bard, A. J.; Faulkner, L. R. *Electrochemical methods*; John Wiley & Sons: New York, 1980.
(50) Trasatti, S.; Editor. *Studies in Physical and Theoretical Chemistry, Vol. 1: Electrodes of Conductive Metallic Oxides, Pt. B.*; Elsevier Scientific Pub. Co.: Amsterdam, The Netherlands, 1981.
(51) Martelli, G. N.; Ornelas, R.; Faita, G. *Electrochim. Acta* **1994**, *39* (11−12), 1551−1558.